Wear 580–581 (2025) 206264

Contents lists available at ScienceDirect

Wear

journal homepage: www.elsevier.com/locate/wear

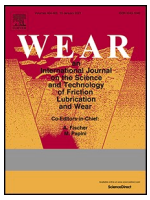

Experimental investigation on the effect of bainite traces on wear and rolling contact fatigue in ER8 railway wheel steel

Angelo Mazzù [a,*], Nicola Zani [a], Candida Petrogalli [a], Ileana Bodini [a], Lorenzo Ghidini [b], Michela Faccoli [a]

[a] University of Brescia, Department of Mechanical and Industrial Engineering, via Branze 38, 25123, Brescia, Italy
[b] LucchiniRS, Via Giorgio Paglia 45, 24065, Lovere, Italy

ARTICLE INFO

Keywords:
Railway wheel steel
Bainite
Wear
Rolling contact fatigue

ABSTRACT

The effect on wear and rolling contact fatigue of dispersed bainitic islands, as a remnant of the production process of railway wheels, is still an open issue. To address this topic, an experimental campaign was carried out on an ER8 steel by means of a small-scale bi-disc machine.

The specimens were extracted at different depths under the tread of a railway wheel, characterized by decreasing hardness and a bainite content. The tests were done in dry rolling-sliding condition, in some cases followed by a wet contact session. Various measurement techniques, including an innovative vision system, were employed to evaluate wear, rolling contact fatigue and surface degradation.

The results showed that, in dry condition, the prevailing damage was delamination wear, whereas, in the wet phase, shelling prevailed. None of the obtained data highlighted a detrimental effect of the bainitic content, in the concentrations considered in this study. This means that a small amount of dispersed bainite can be tolerated, reducing energy consumption, material waste and cost in the production process.

1. Introduction

Nowadays, hypoeutectoid carbon steels are largely employed in the production of many typologies of railway wheels, especially for high-speed applications. In Europe, the EN-13262 ER8 steel is mainly used for wheels of high-speed passenger trains with Electric Multiple Units (EMU) traction system. Over time, the initial steel has been improved, in the respect of the standard prescriptions, by optimising the control of chemical composition, inclusion content, forging and rolling process and thermal treatment [1].

The forging and rolling process is preceded by a pre-heating phase up to 700 C–900 C; subsequently, the forging is obtained by multiple steps. Then, the resulting microstructure is optimized by means of a rim-chilling and a subsequent tempering. During the rim-chilling, the microstructure is first completely austenitized by heating the forged component up to about 900 C and keeping that temperature for the time necessary; subsequently, the manufact is cooled with different rate, depending on the zone. The microstructural evolution of the ER8 steel grade is described by its Continuous Cooling Transformation (CCT) diagram, which illustrates the phase transformations occurring during cooling. Fig. 1 shows the CCT diagram of the steel investigated in the present study, which was preliminarily obtained through experimental testing using a LINSEIS L78 RITA dilatometer. Rapid cooling leads to the formation of martensite, which is characterized by very high hardness. In the subsequent region, where the cooling rate is still relatively high but lower than that required for martensitic transformation, bainite forms within the ferritic-pearlitic microstructure. Although this bainitic region is minimized through carefully designed steel chemical composition aimed at reducing bainite formation, its presence remains almost inevitable [1]. The subsequent tempering treatment, consisting in heating the manufact up to about 600 C, keeping such temperature for the necessary time and chilling at low rate, increases the amount of globular pearlite to optimise ductility and toughness; however, it cannot remove the bainitic islands, which remain, in traces, especially near the tread. For this reason, a machining allowance is typically left on the raw wheel, dimensioned to ensure that most of the bainite formation is confined to a region that will later be removed.

Concerning bainitic steels for railway wheels, some studies highlighted better performances against various damage phenomena. For instance, Miranda et al. found that bainitic steels are more resistant than

* Corresponding author.
E-mail address: angelo.mazzu@unibs.it (A. Mazzù).

https://doi.org/10.1016/j.wear.2025.206264
Received 7 May 2025; Received in revised form 1 July 2025; Accepted 18 July 2025
Available online 19 July 2025

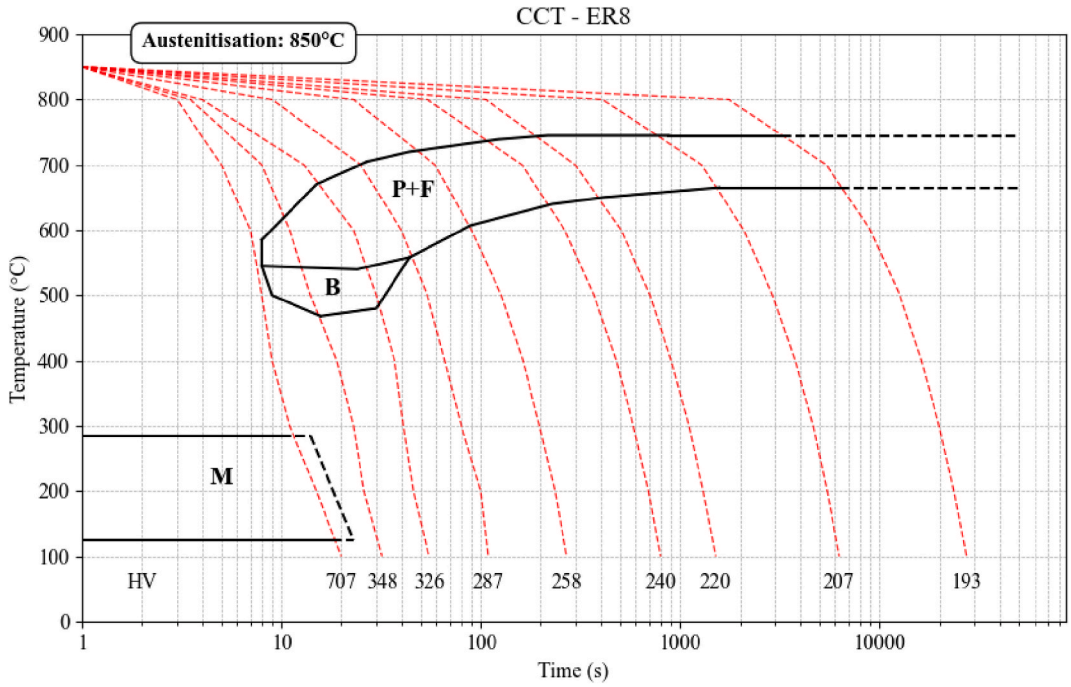

Fig. 1. Experimentally obtained Continuous Cooling Transformation (CCT) diagram of the studied ER8 steel grade.

pearlitic ones to wear and crack propagation [2]. Zhou et al. [3] found that the increase of the wear resistance is associated to the higher thickness of the surface hardened layer. Sharma et al. [4] found that bainitic steels offer a better performance in terms of wear resistance thanks to the increased hardness and strength. Conversely, other studies highlighted a worse wear resistance in steel with high bainitic content. Li et al. [5] measured a higher wear rate in an ER8 steel with a high bainite content (50 %) compared to the same steel with a fully ferritic-pearlitic microstructure, which was less hard. The detrimental effect of a high bainite content (68 %, as estimated using Image-Pro Plus software) within the ferritic-pearlitic microstructure of ER8 steel on its RCF behavior is also confirmed by Gao et al. [6] who reported a RCF limit for the bainite-containing microstructure lower than that of a completely ferritic-pearlitic microstructure. Zhang et al. [7] found that the bainite phase is associated with an increase of the plastic strain and wear rate, in steels with 80 % content of upper bainite.

The results above concern the effect of a high content of bainitic structures in the steel (more than 50 %), intentionally achieved; however, the effect of dispersed bainitic islands in a ferritic-pearlitic matrix, which remain as a remnant of the production process, is still an open issue that was investigated by few authors. Babachenko et al. [8] found that the presence of bainitic islands (up to 16 % in volume fraction) is correlated with a decrease of the fracture toughness; however, these results were obtained by means of tensile stress and fracture mechanics experiments and the effect on wear and RCF could not be determined. Gao et al. [6], by means of analyses on used wheels, found that bainitic islands favour crack nucleation and propagation; however, they could not measure wear and RCF in controlled environmental conditions. Suetrong and Uthaisangsuk [9] found that bainitic islands enhance crack nucleation but slow down crack propagation; however, again, the results were not obtained by rolling contact experiments and the typical damage mechanisms occurring in this condition were not evaluated. Zani et al. [10] showed that the bainitic islands in an ER8 steel can increase the plastic deformation around them, but this phenomenon can be neglected if their concentration is less than 11 %; however, this study is purely numerical and needs experimental validation.

In the industry, the mismatch between the mechanical properties of the bainitic islands and the surrounding matrix is considered a non-favourable factor in terms of wear resistance: this is the main reason for which many efforts have been done to decrease concentration of bainitic phase by improving the production process. To obtain this, the rim chilling was calibrated to confine most of the bainitic structures in the outer layer of the tread, which has to be subsequently removed in the final turning phase.

Notwithstanding these improvements, steels with no traces of bainite are required in some important markets. Given current technological limitations, achieving this objective necessitates increasing the thickness of the material removed during machining, which leads to higher energy consumption and production costs. In addition, the layer of material with the best mechanical properties is wasted. Therefore, it is crucial to verify whether a low concentration of bainitic structures really affects the steel performance in terms of resistance to wear and fatigue.

To face this issue, an experimental campaign was done by means of a small-scale bi-disc machine. This experimental method was successfully used in the past to characterise the response of wheel and rail steels to repeated contact loads, especially in terms of wear, ratcheting and fatigue. In particular, it was shown that rolling-sliding contact in dry condition is especially useful to characterise the wear and ratcheting behaviour, whereas the alternation of dry and wet contact usually enhances fatigue crack propagation [11–15]. For these reasons, in the present work it was chosen to make tests with an initial session in dry condition to characterise the wear behaviour, followed by a session in wet contact to characterise the fatigue response. In addition, some tests in dry condition only were done to observe their effect in the subsurface layer by means of destructive tests. The specimens were extracted from a real wheel at different depths, characterised by varying hardness and concentration of dispersed bainite, to verify their role in the damage phenomena. The investigated layer was thicker than that normally exploited in operation, starting from the allowance and exceeding the end-of-life depth, to explore the possibility of extending the thickness of the useable layer in real applications.

Table 1
Chemical composition and mechanical properties of wheel and rail steels.

		ER8	900A
Chemical composition [wt%]	C	0.55	0.77
	Mn	0.75	1.02
	Si	0.37	0.33
	S	0.002	0.015
	P	0.015	0.019
Ultimate tensile strength [MPa]		956	910
Yield strength [MPa]		596	475
Elongation [%]		17	15
Brinell hardness [HB]		283	271

2. Materials and methods

2.1. Materials

The present study focuses on the ER8 steel grade for railway wheels, provided by Lucchini RS. This steel is tested against UIC 900A rail steel, a commonly used pearlitic rail steel grade. The chemical composition and mechanical properties of both steel grades, shown in Table 1, were determined using an optical emission spectrometer (ARL iSpark 8860) following the ASTM E415 and EN13262 standards.

Samples for the rolling contact fatigue tests were extracted from four different depths from the tread of a raw wheel, designated as A, B, C, and D, as shown in Fig. 2. The samples were cylindrical discs with a thickness of 15 mm, a diameter of 60 mm and correspond to four specific microstructural conditions, each representing varying bainite percentages. Depth A primarily resides within a mechanical allowance layer of 17.5 mm, which is subsequently removed in the final wheel product. Depths B and C, however, fall within the functional thickness of the wheel, extending up to the regulatory wear limit of 35 mm. Depth D, positioned beyond this functional region, allows for further analysis of deeper material properties.

Fig. 3 shows the microstructure of ER8 steel at increasing depth from the tread, with the bainitic islands highlighted. The sampling depth is identified by the textbox at the up-left corner of each picture. A transition from a bainitic-ferritic-pearlitic microstructure at the shallower depths (A and B) to a fully ferritic-pearlitic one at greater depths (C and D) is shown. Specifically, at depth A, the bainite content decreases from 11.93 % near the surface to a value between 0.76 % and 0 % as the distance from the tread increases. A similar trend is observed in depth B, where the bainitic phase further decreases from values within the same range (between 0.76 % and 0 %) down to 0 % at the end of the layer.

This variation is a direct consequence of the heat treatment, which induces a gradual reduction in hardness with increasing depth. As illustrated in Fig. 4, the results confirm the expected decline in hardness as the amount of bainite decreases and the microstructure becomes progressively coarser. At greater depths (positions C and D), where bainite is no longer present, hardness variations persist due to the residual effects of the rim-chilling heat treatment. In the near-surface region (from 7.5 mm to 22.5 mm), a finer spacing of measurement points was adopted to capture the sharp local hardness variations associated with the non-uniform distribution of bainite. Beyond this region, where the microstructure transitions to a uniform ferrite-pearlite mixture and bainite is completely absent, a wider spacing was used, as no significant local hardness fluctuations were expected.

These sample extraction zones provide an ideal framework for evaluating the influence of different metallurgical conditions on rolling contact fatigue and wear performance of ER8 wheels. In addition to the wheel samples, rail specimens made of 900A steel were extracted from the head of actual rails, with their axes perpendicular to the rolling direction, to ensure mechanical properties as close as possible to real operating conditions. Both the wheel and rail samples share the same geometry, which will be further detailed in the following section.

2.2. Rolling contact tests

The rolling contact tests were conducted using a bi-disc testing machine to evaluate the tribological behavior of selected wheel steels in both dry and subsequent dry – wet conditions against rail steel. A schematic of the test rig is shown in Fig. 5: it consists of two independently driven shafts, each holding a cylindrical specimen, with one shaft mounted on a movable carriage. A hydraulic piston applies the normal load to generate the desired contact pressure, while a torque sensor continuously monitors the tangential force, which is adjusted using a correction algorithm to eliminate internal friction effects within the machine. More details on the bi-disc test bench and its measurement systems are given in Ref. [13].

The tests were divided into two categories: dry test and tests with a dry session followed by a wet one (identified as “dry + wet” in the following). In dry tests, samples underwent cyclic loading at 1100 MPa stress and a 1 % slip rate for 50,000 cycles. In dry + wet tests, after the dry phase, further 20.000 cycles were done with a jet of water on the contact zone, added with 10 % glycol to prevent corrosion of the machine parts. The repeatability of the tests in dry condition was checked by comparing the non-destructive measurement results of the dry tests with those of the dry phase of the dry + wet tests.

Before the tests, all specimens were ultrasonically cleaned and rinsed

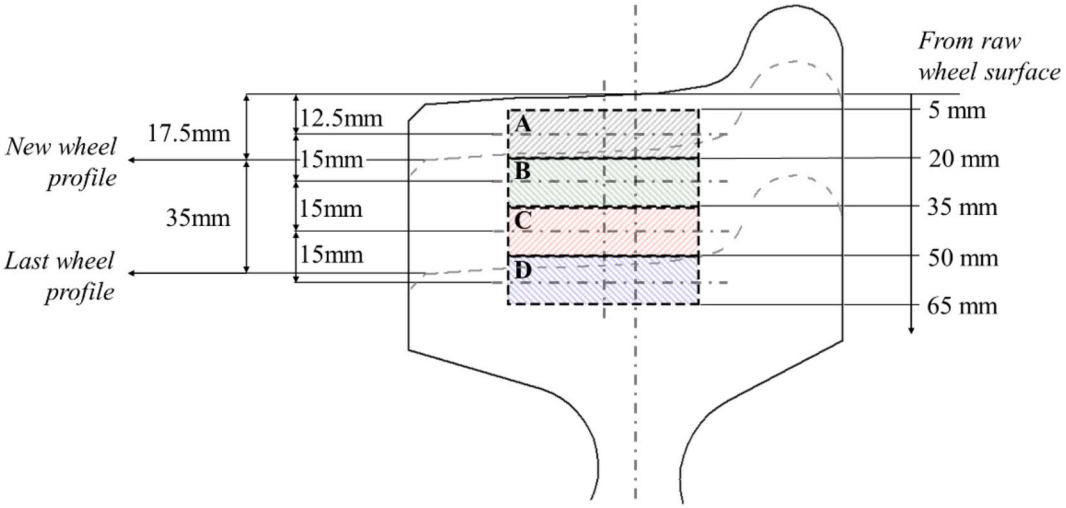

Fig. 2. Schematic sampling scheme from the raw wheel (A, B, C, and D).

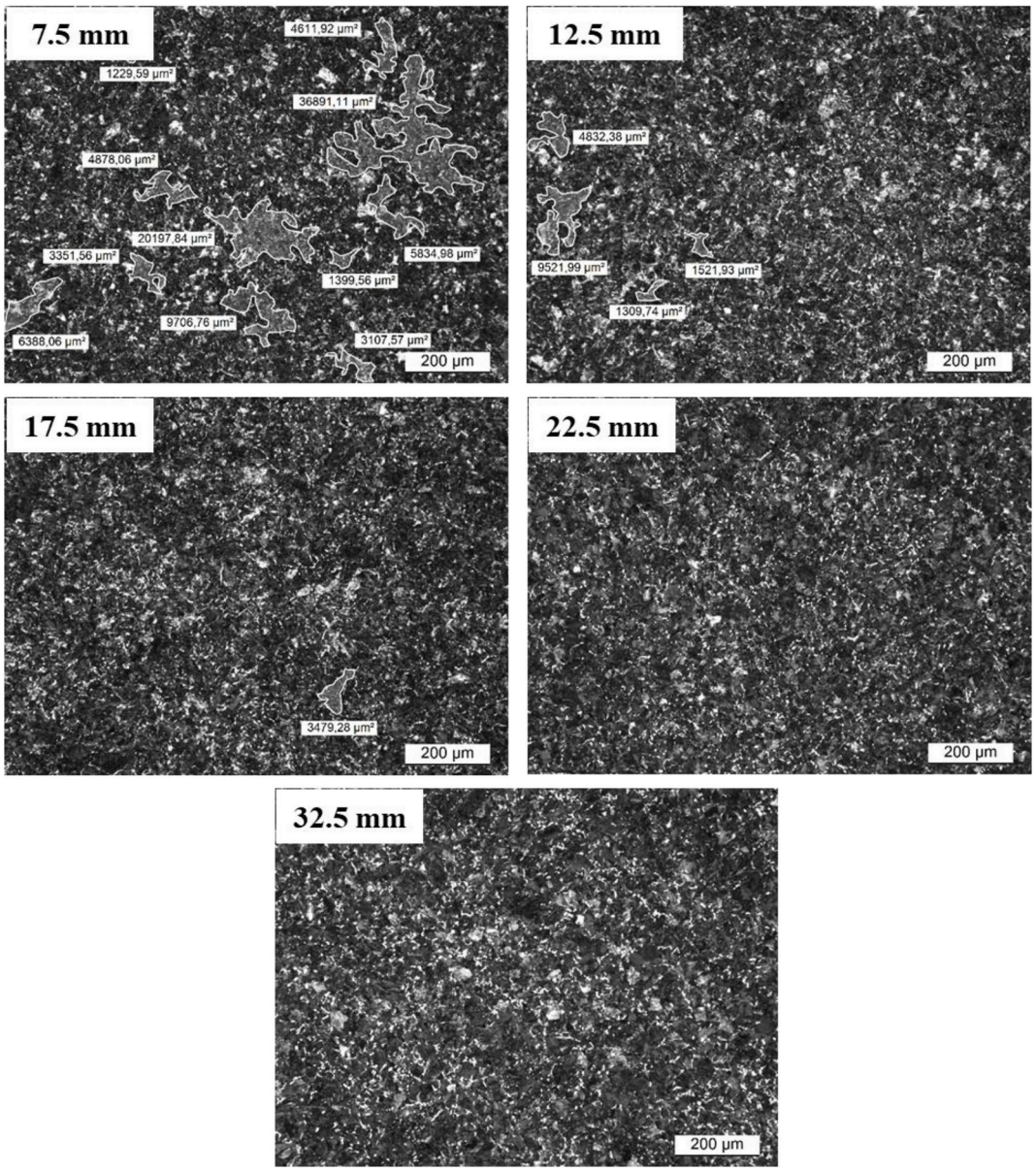

Fig. 3. Microstructure from the raw surface of the wheel tread with highlighted bainite at increasing depth from the surface (7.5 mm–32.5 mm).

to prevent the formation of oxides and weighed using a precision balance with a resolution of 0.001 g. The testing procedure included periodic stops for contact surface observation and weight measurements. After each stop, the specimens were cleaned again, weighed, and the profile of the rolling surface was measured using WENGLOR MLWL171, a laser triangulation sensor designed for precise, non-contact 3D surface profiling. At each measurement about 180 profiles were acquired, with 2.048 points per profile. The quadratic roughness R_a of each profile was calculated, from which the average R_a of the whole specimen surface was determined. More details on the measurement method are given in Ref. [16].

To assess the contact surface state, a vision system was used, about which full details can be found in Refs. [17–20]; here, an extreme synthesis of the method is given. The contact surface of the specimens was illuminated by two defocused laser pointers, to produce a diffused light. A portion of this surface was acquired by a high-speed camera (PROMON 501; AOS Technologies AG) every 5000 cycles; an overall picture of the surface state was obtained, characterized by lights and shadows that could be correlated to crests and dips on the surface, with brighter areas corresponding to the bottom of surface pits. The acquired images were binarized: after choosing a proper threshold for the level of grey, all the pixels were changed into black or white if their level of grey was lower or higher than the threshold, respectively. After that, groups of white pixels that could be enclosed by a continuous line were identified as blobs, and each blob was assumed as the image of a surface pit. The blob analysis allows obtaining several parameters aimed at evaluating the surface state; in the present paper, the following ones were considered the most significant:

- A_B, defined as the average area of the blobs detected along the contact surface;
- R_B, defined as the ratio of the total area of the detected blobs to the overall contact surface area.

The former is an index of the size of the pits, whereas the latter expresses the rate of the damaged surface. At the end of the tests, after cleaning and weighing, the damage of the wheel sample rolling surface was assessed using a DMS 300 stereomicroscope equipped with a Leica digital camera and LAS 4.13 image analyzer software, just before sectioning the samples. The wheel discs were sectioned along the mid-

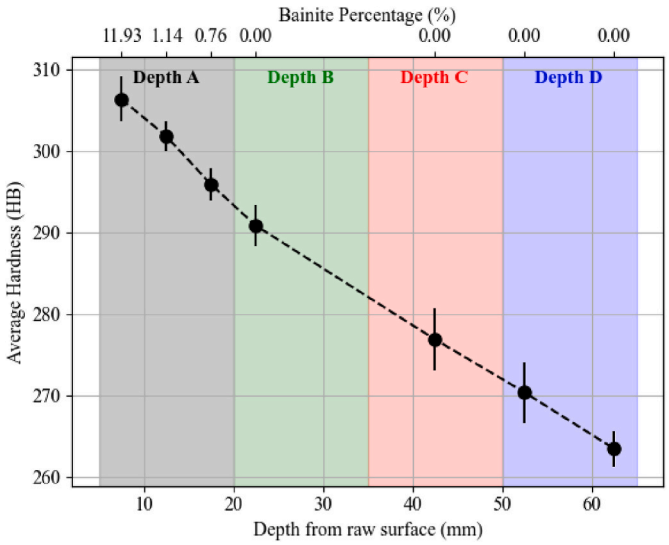

Fig. 4. Bainite content variation and hardness values as a function of depth from raw wheel surface.

plane, orthogonally to their axis. The sample cross-sections were then ground with silicon carbide abrasive papers (grades from 80 to 1200) and polished with polycrystalline diamond pastes (3 μm and 1 μm). Vickers hardness measurements were taken, using a Mitutoyo HM-200 hardness testing machine, under a 1000g load applied for 15 s, at varying distances from the contact surface to assess strain hardening and determine the depth of the deformed layer. Finally, the samples were observed both with and without 2 % Nital etching (2 vol % HNO_3 in ethanol) using a Leica DMI 5000 M light optical microscope, allowing for the examination of crack initiation, propagation, and microstructural changes.

3. Experimental results

The experimental results primarily focus on the wheel specimens, as the objective of the investigation is to assess the effect of varying bainite content in ER8 steel on wear and rolling contact fatigue behavior. However, wear results are also reported for the rail specimens to evaluate the effect of the driver (rail sample) or follower (wheel sample) role in the coupling, which is evident especially in the wet phase.

3.1. Coefficient of friction

Fig. 6 shows the coefficient of friction recorded in all the tests. A general trend can be identified. After an initial run-in period that can vary from a few hundred to 20,000 cycles, the coefficient of friction tended to settle to a value between 0.30 and 0.35 in dry condition and around 0.05 in wet condition. In the run-in period the coefficient of friction is lower than in the stabilized condition. The reason is unknown; a hypothesis is that the specimens started from varying conditions of oxidation on the surface. Indeed, oxides casually formed on the contact surface tend to lower the coefficient of friction; therefore, the specimens could start the test with varying oxidation state and, consequently, the coefficient of friction in the initial phase could vary. However, once the oxidized layer was removed, the coefficient of friction tended to be stabilized and uniform for all specimens. Therefore, to characterise the wear behavior of the specimens it was decided to exclude the initial 20,000 cycles in all the tests.

3.2. Wear

Fig. 7 shows the wear curves obtained from the tests conducted on the samples taken at the four different depths, paired with the rail samples. It can be observed that, at the same extraction depth, the test results in terms of sample weight loss are very similar, demonstrating the repeatability of the tests. At all depths, the curves exhibited an initial slight mass loss, characteristic of the run-in phase. According to Lewis and Dwyer-Joyce [21], this low mass loss is due to the accumulation of plastic deformation on the contact surface caused by the applied load from the very first cycles. During this period, the rolling surface material undergoes accommodation and surface roughness is gradually smoothed out, marking the incubation period of the wear mechanism. The run-in phase is followed by a phase where the slope of the curves increases and can be approximated by a linear function. In this region, the wear phenomenon reaches a steady-state regime, consistent with the stabilization of the friction coefficient shown in Fig. 6, allowing the calculation of the wear rate. This was calculated both in terms of weight loss per

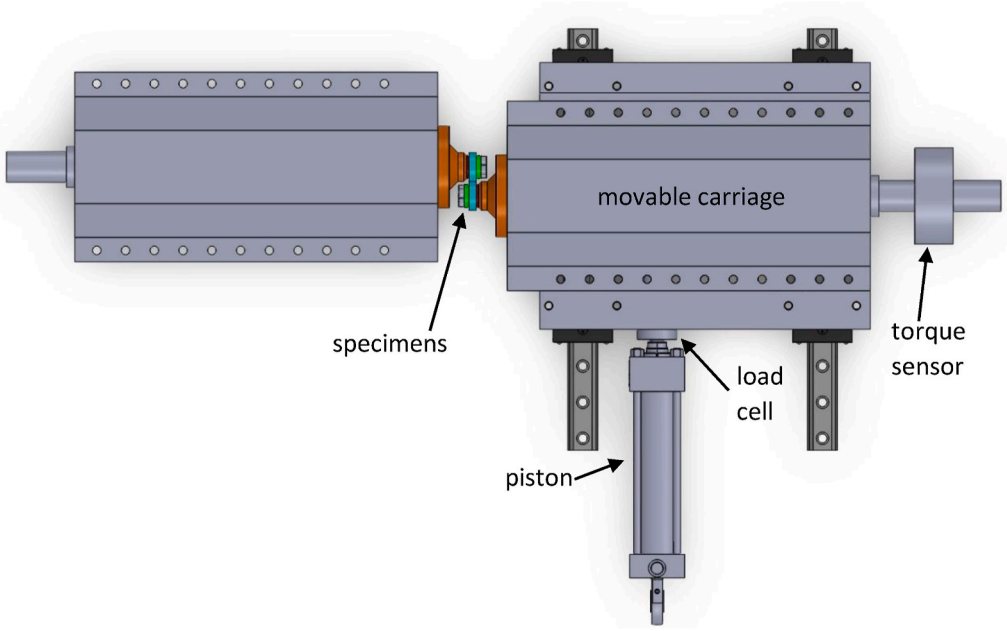

Fig. 5. Schematic of the bi-disc machine.

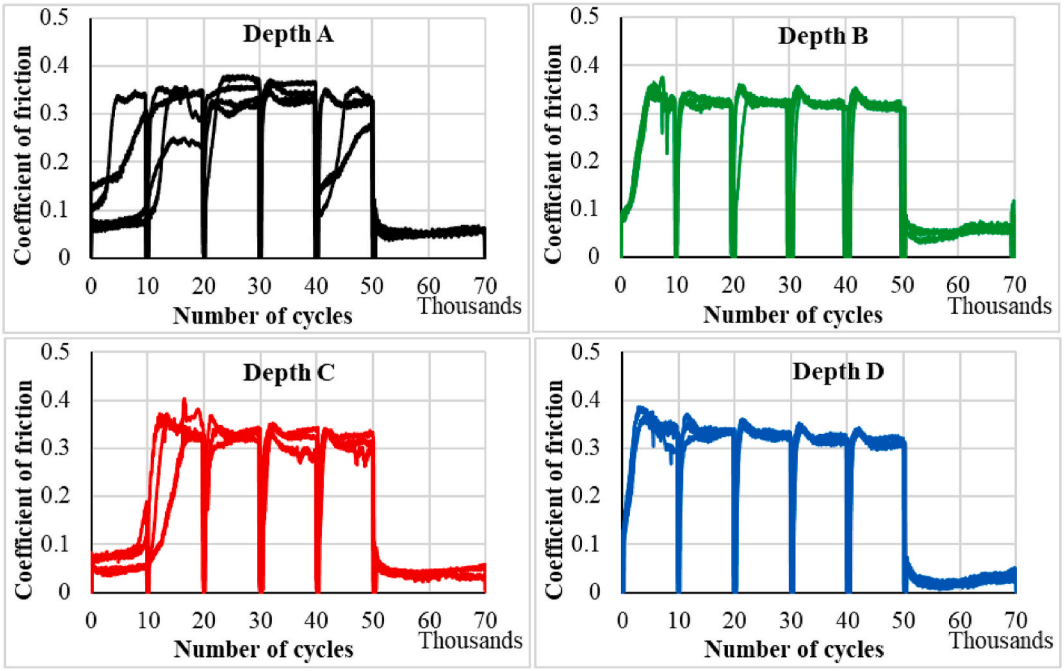

Fig. 6. Coefficient of friction in all the tests.

cycle, as well as in terms of wear number K, defined as follows according to the Archard model:

$$K = \frac{\Delta V \cdot H}{F \cdot \Delta s} \quad (1)$$

where:

- ΔV is the worn volume per cycle;
- H is the Brinell hardness of the softer material, that in the present work was the rail steel (see Table 1);
- F is the normal contact load;
- Δs is the sliding distance per cycle.

As presented in Table 2, the wear rate of the wheel steel samples increases with increasing extraction distance from the rolling surface of the wheel. This is due to the decrease in steel hardness as the distance from the tread increases (as shown in Fig. 4), a consequence of the heat treatments applied to the wheel during the manufacturing process. Therefore, the presence of small amounts of bainite (up to around 12 % at extraction depth A) within the ferritic-pearlitic microstructure of ER8 steel contributes to increasing the hardness and consequently its wear resistance under the dry contact condition. With regard to the rail steel samples, their wear rate is always lower than that of the wheel samples and no significant variations are observed in their wear rate values with different extraction depths of the paired wheel samples. The obtained wear number, in all the tests, fell in the range correlated to "mild wear" according to several wear maps [22–24]. Finally, for tests that included the wet phase, a third region can be observed, where the presence of the liquid reduced friction at the contact between the samples (see Fig. 6), influencing the progression of the damage, as will be evident from the results of the microscope analysis.

Fig. 8 shows the weight loss in the wet phase of the dry + wet tests. The weight loss is much higher in the wheel specimens than in the rail ones. This is due to the crack propagation enhanced by the entrapped fluid effect, which occurs in the follower only (wheel specimen), owing to the orientation of the surface cracks generated in the dry session, as described by Mazzù et al. [15]. With respect to the results obtained in the dry phase, there is much more dispersion in the wet phase, but this is consistent with the fact that fatigue, which is a much more aleatory phenomenon than wear, prevails. A clear trend that can be related to the increasing depth of the specimen extraction cannot be recognized in the wet session.

3.3. Contact surface characterization of the wheel steel samples

Fig. 9 shows the quadratic roughness R_a measured in the dry step of all tests on the wheel specimens. As a general rule, the roughness tends to stabilize after the initial 10,000–20,000 cycles. The highest average stabilized quadratic roughness is recorded in the B specimens, the lowest in the D ones. This trend is consistent with the behavior of the coefficient of friction, whose stabilization approximately coincides with the stabilization of the roughness value.

Fig. 10*a* shows the R_B parameter, which is an index of the general pitting of the contact surface, during the tests run in dry condition only. Again, in general an increment of the contact surface damage indexes can be identified after the initial run-in period; after that, the variations of the indexes are lower, tending to oscillate around an average value. Whereas the A, B, and C specimens tend to similar damage index, the D specimens exhibit a higher stabilized R_B. Fig. 10*b* shows the A_B parameter, which is an index of the average size of the pits. Even this parameter increases and stabilizes after the run-in period. In this case, the A and B specimens have a stabilized A_B value lower than the C and D ones, meaning that in the latter the average size of the pits is larger. These data show that, in general, the damage indexes are higher in the specimens taken in the deeper layers, suggesting that the damage increases as far as the surface hardness decreases.

3.4. Microscopic analysis of the contact surface and cross-section of the wheel steel samples

Fig. 11 presents representative stereomicroscope micrographs of the damage observed on the contact surface of the wheel steel samples taken at depth D, where the most severe damage occurred, at the end of the dry (Fig. 11a) and dry + wet (Fig. 11b) tests. Regarding the damage mechanisms, all samples exhibited both wear and rolling contact fatigue (RCF), which were subsequently analyzed in greater detail at higher magnifications on the sample cross-sections. It is well-established that

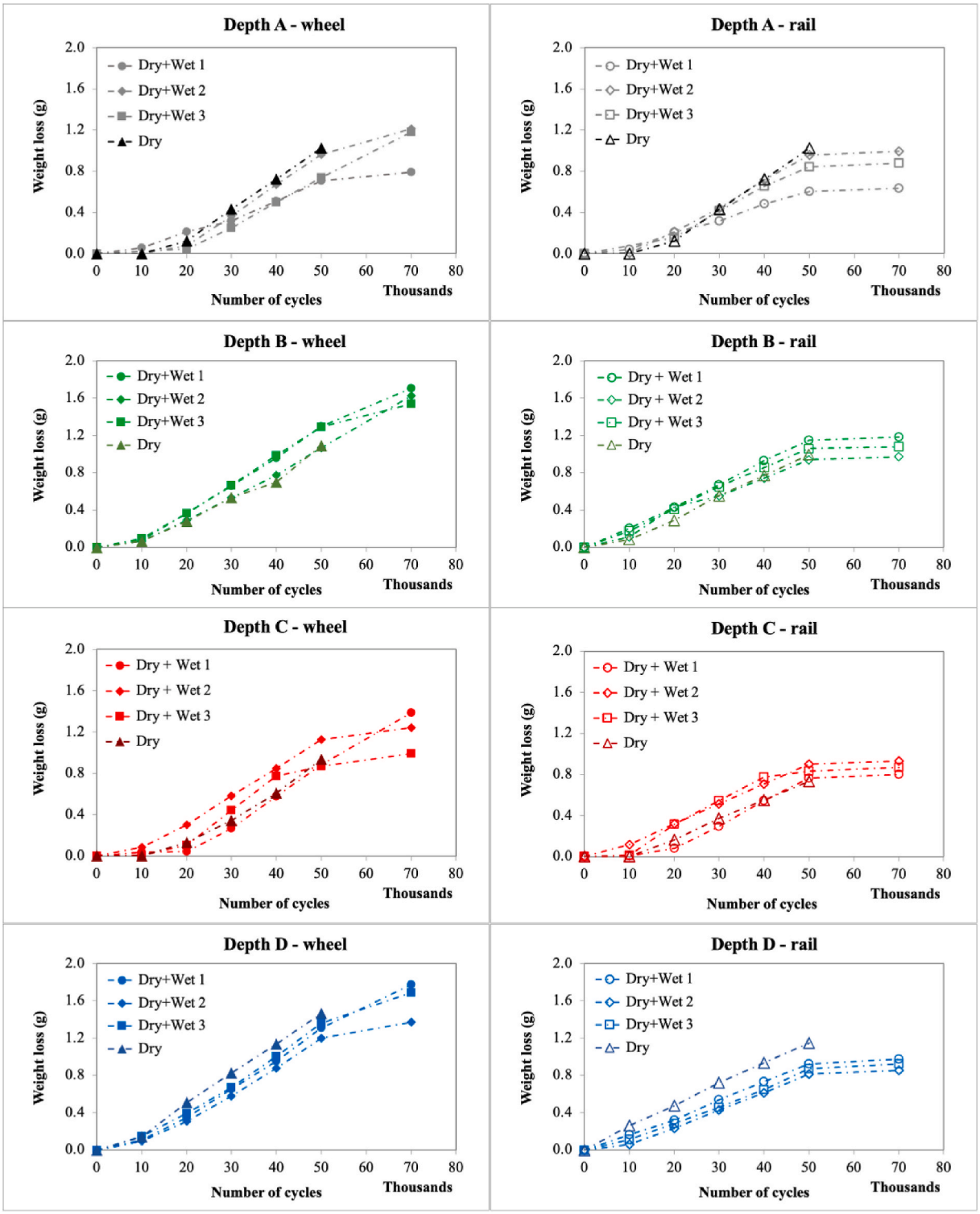

Fig. 7. Wear curves of the wheel and rail steel samples at different extraction depths of the wheel steel samples.

there is often competition between these two damage phenomena [11,25,26], which are typical of railway wheels. When wear predominates, there are fewer RCF cracks, as wear tends to remove these surface cracks. Conversely, when RCF predominates, there is a greater amount of cracking. In the samples tested under the dry condition, delamination was the predominant damage mechanism, whereas those tested under the dry + wet condition exhibited significantly more severe shelling damage. Both damage mechanisms are more clearly visible in the cross-sections of the samples and will be discussed in relation to them.

Fig. 12 shows representative optical micrographs of the damage observed in the cross-section of the wheel steel samples, taken at the four investigated depths, at the end of the dry tests. In all samples, just below the contact surface, the microstructure appears plastically deformed in the direction of the surface friction. Furthermore, short surface-initiated cracks were observed, propagating at a slight inclination with respect to the surface, following the plastic flow and remaining confined within the plastically deformed layer. The observed damage is caused by the fatigue mechanism known as “ratcheting”: the accumulation of plastic

Table 2
Average wear rates and wear numbers of the wheel and rail steel samples.

Sample extraction depth	Average wear rate (g/cycle)		Average wear number K	
	Wheel sample	Rail sample	Wheel sample	Rail sample
A	2.47×10^{-5}	2.08×10^{-5}	5.96×10^{-5}	5.02×10^{-5}
B	2.71×10^{-5}	2.15×10^{-5}	6.53×10^{-5}	5.18×10^{-5}
C	2.79×10^{-5}	2.26×10^{-5}	6.73×10^{-5}	5.45×10^{-5}
D	3.03×10^{-5}	2.00×10^{-5}	7.31×10^{-5}	4.82×10^{-5}

deformation on the sample surface under cyclic loading promotes the nucleation of surface cracks, their propagation beneath the surface and the consequent delamination process, i.e., the detachment of material fragments [12,14,27]. Regarding crack nucleation and propagation, Liu et al. [28] reported that in D2 wheel steel these cracks originate from the proeutectoid ferrite and the ferrite lamellae within the pearlite. Since proeutectoid ferrite has lower mechanical strength than pearlite, it creates a weak interface that facilitates crack propagation. This behavior also occurs between the ferrite and cementite lamellae within pearlite due to the difference in their mechanical strengths. The same mechanism was observed by Hu et al. [29] in ER7 and CL60 wheel steels, where the high ferrite content contributed to crack formation and propagation. This phenomenon can also be considered plausible in ER8 steel due to its similar microstructure. Regarding the material fragments generated, they act as a third body in the contact between the two samples during the test, promoting the wear phenomenon [29,30]. They may also

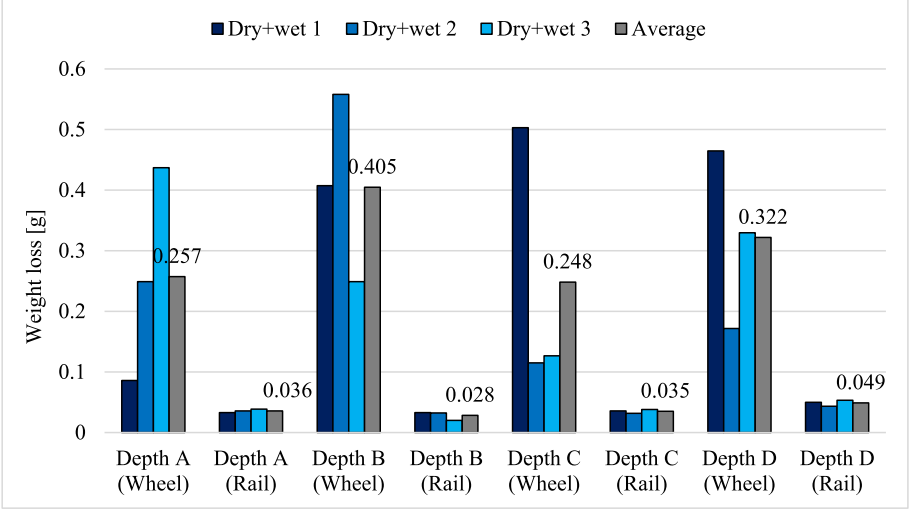

Fig. 8. Weight loss in the wet phase of the tests for wheel and rail samples, in the single tests (blue histograms) and averaged (grey histograms). (For interpretation of the references to colour in this figure legend, the reader is referred to the Web version of this article.)

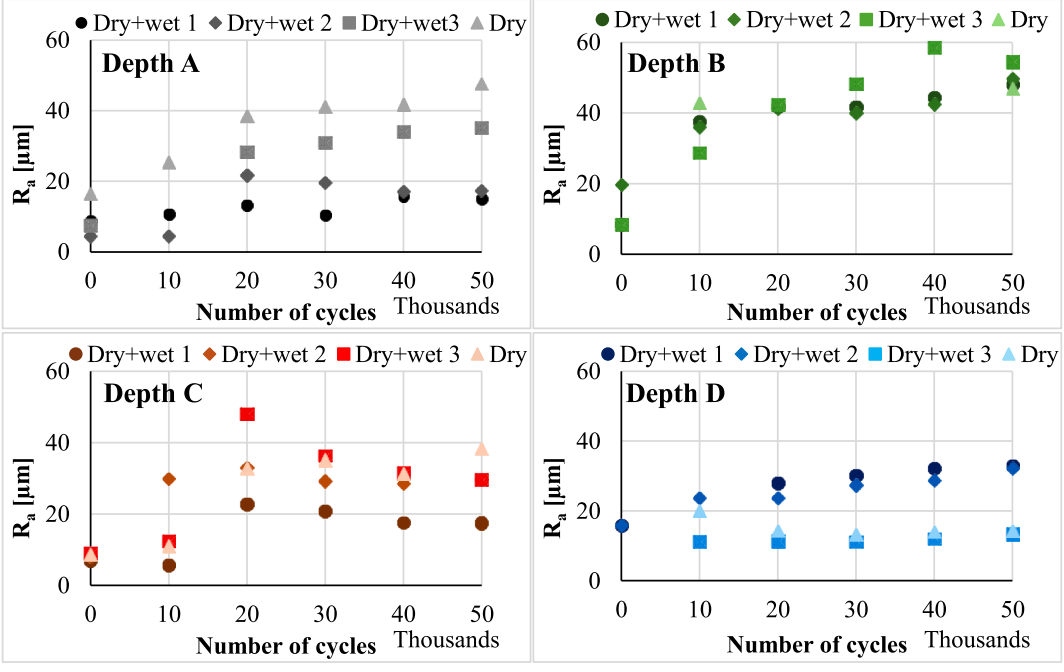

Fig. 9. Average quadratic roughness R_a of the wheel specimens in all the tests.

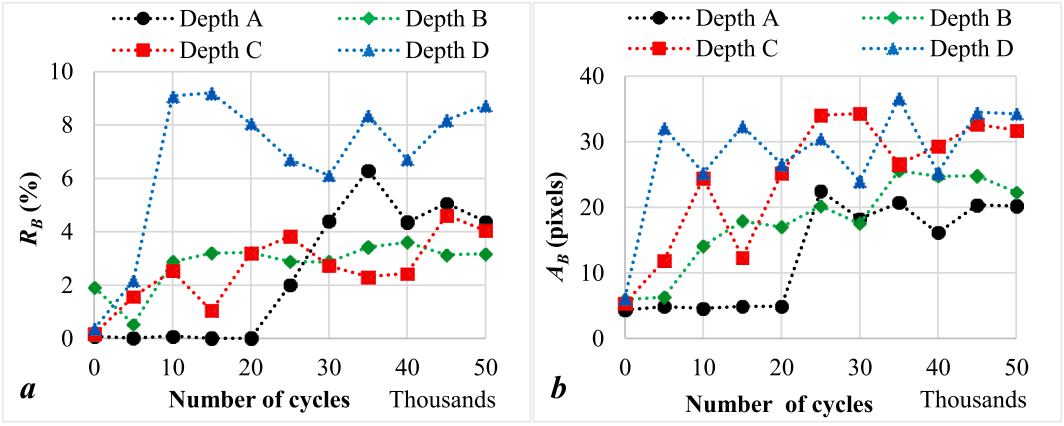

Fig. 10. Surface damage indexes in the tests run in dry condition: a) percentage damaged area; b) average blob area.

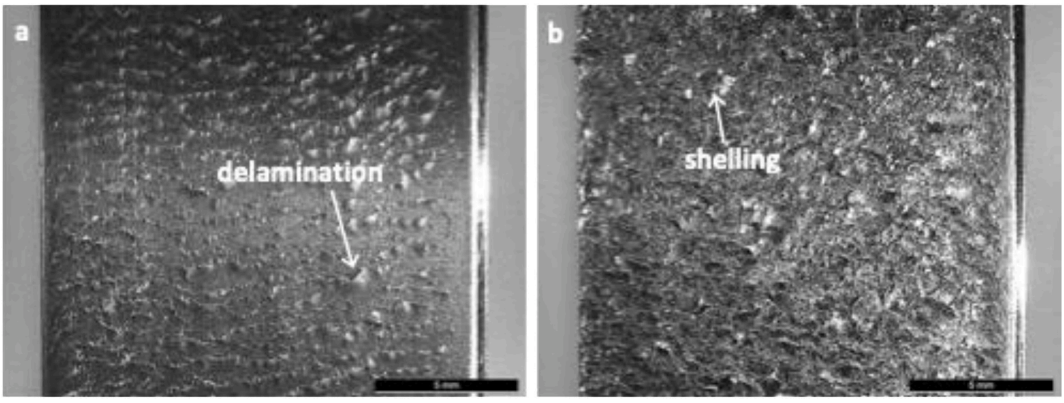

Fig. 11. Micrographs of the contact surface of the wheel steel samples at the extraction depth D at the end of dry (a) and dry + wet (b) tests.

become trapped within RCF cracks, as shown in Fig. 12 and as also reported by Hu et al. [29]. These observations are consistent with the results obtained from the wear curves presented in Section 3.2, which indicated a progressive weight loss of the wheel steel samples during the dry step. It is worth noting that the average weight loss of the samples at the end of the dry phase, as well as the wear rate, is lower for those extracted at depth A, which has the highest bainite content among all depths. This is consistent with the greater hardness of the material at depth A compared to the other depths, leading to enhanced resistance to wear and RCF under the dry contact condition.

In the dry tests delamination wear appeared as the prevailing phenomenon, because no deep crack propagation with detachment of shells was observed. On the other hand, in the mixed tests, when, after the first 50,000 dry cycles, the samples were subjected to 20,000 cycles in the presence of water, severe shelling clearly emerged as the primary damage mechanism. This was expected, as wet conditions have been widely recognized as a factor that reduces wear while significantly exacerbating RCF phenomena because of the entrapped fluid pressurization [13–15,31–33]. Fig. 13 shows significant optical micrographs of the damage sustained by the wheel steel samples taken at the four investigated depths. The damage was consistent across all depths, both in nature and, apparently, in extent. The pumping effect of the liquid present in the contact zone between the two samples during the test caused an acceleration in the propagation of the cracks formed during the dry phase. Moreover, these cracks exhibit a characteristic branching effect and tend to merge, leading to the onset of shelling, which results in significant material detachment. The same damage mechanisms were observed in ER8 steel tested under dry + wet conditions by Faccoli et al. [14], closely resembling the typical wheel tread damage found on ER8 wheels of a Swedish train in service [34]. The finding aligns with the substantial increase in sample weight loss measured at the end of the wet phase, as detailed in Section 3.2.

3.5. *Subsurface hardness of the wheel steel samples*

Fig. 14 presents the Vickers hardness measured on the cross-sections of the wheel steel samples at the end of the tests, plotted as a function of depth beneath the contact surface, aiming to assess the degree of work hardening and determine the depth of the deformed layer. An increase in hardness is observed in the region closest to the contact surface for all samples, with the maximum value occurring just below the contact surface, where the maximum orthogonal shear stress is present. This result aligns with the deformation pattern observed metallographically (Figs. 12 and 13), as the progressive accumulation of plastic strain beneath the contact surface leads to material hardening.

These hardness profiles are also consistent with findings from previous research on various railway steels, obtained through bi-disc laboratory tests [5,13,14,29,35] under dry conditions and under dry + wet conditions [13,14]. The highest hardness values are obtained in the samples tested under the dry condition. In particular, the maximum hardness was recorded in the sample taken at depth D (HV1 = 444), where the steel exhibits the lowest initial hardness (HV1 = 266) and, therefore, shows the highest work hardening capacity (ΔHV1 = 178). This result is consistent with the findings of Yokoyama et al. [36], who assert that the lower initial hardness of pearlite facilitates work hardening. Conversely, the smallest increase in hardness was observed in the sample taken at depth A (maximum HV1 = 341, initial HV1 = 300, ΔHV1 = 41). Regarding the depth of the deformed layer, the samples taken at depths C and D exhibit the greatest values, measuring 0.4 and 0.5 mm, respectively. This demonstrates the greater deformability of the

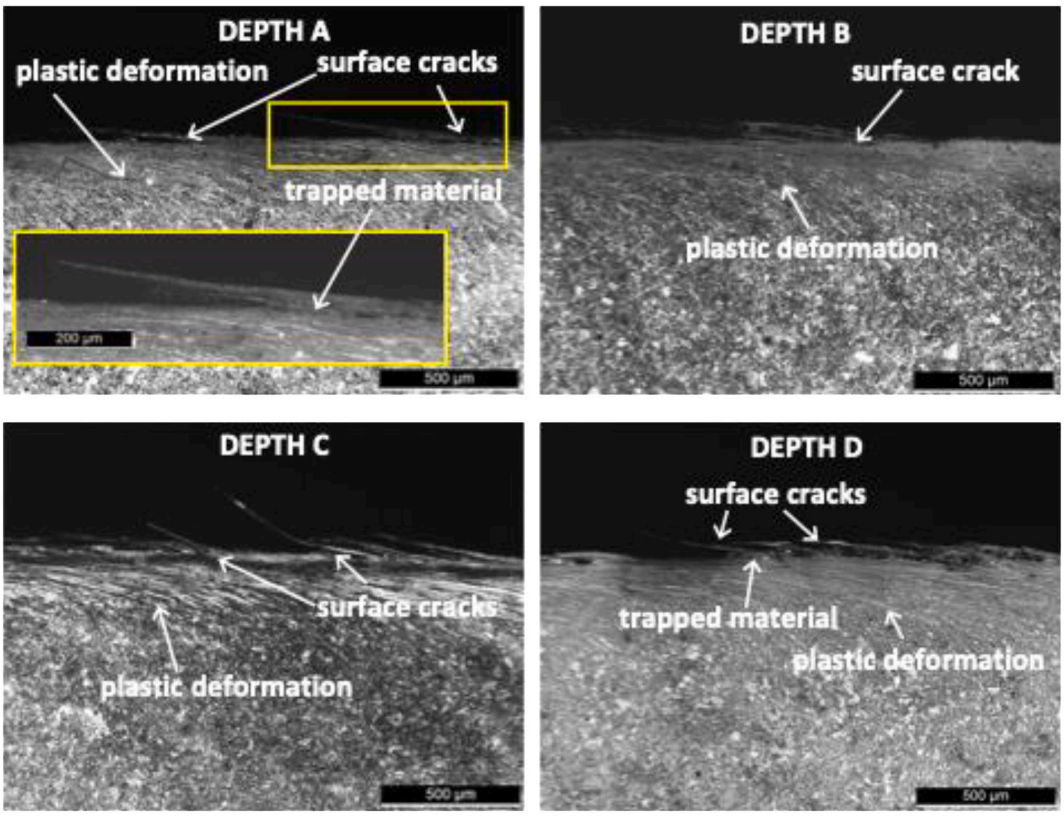

Fig. 12. Micrographs of the cross-section of the wheel steel samples at the different extraction depths at the end of the dry tests.

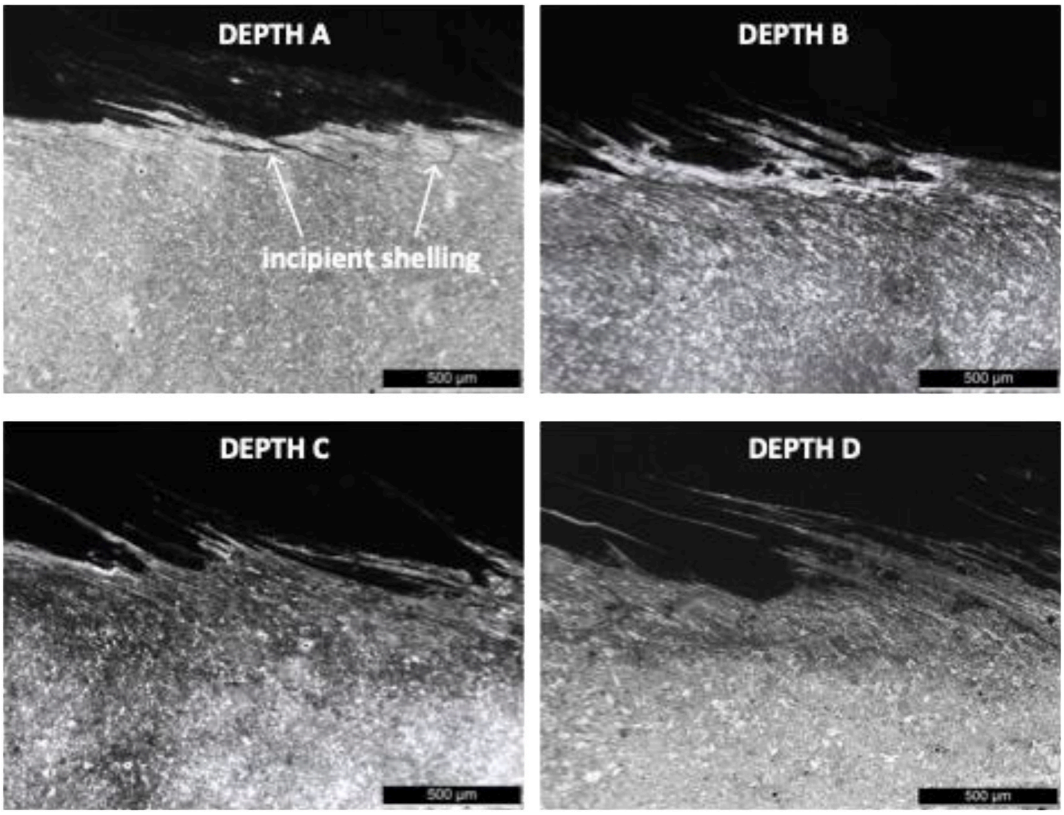

Fig. 13. Micrographs of the cross-section of the wheel steel samples at different extraction depths at the end of the dry + wet tests.

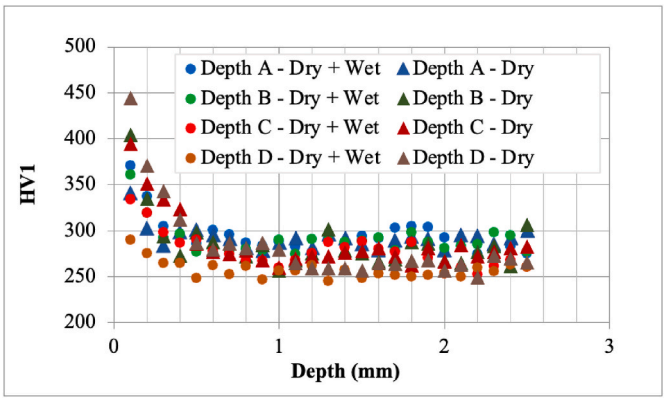

Fig. 14. Vickers hardness profiles on the cross-section of the wheel steel samples at the end of the tests.

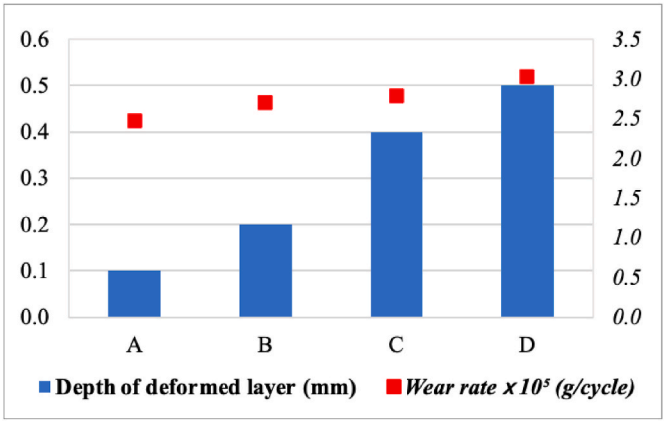

Fig. 15. Correlation between the depth of the deformed layer and wear rate of the samples at different extraction depths of the wheel steel samples.

fully ferritic-pearlitic microstructure compared to that containing traces of bainite. Regarding the samples from the mixed tests, at the same extraction depth, the maximum measured hardness value is always lower than that of the dry tests due to the significant material detachment, which has removed the most work hardened layer.

4. Discussion

The results obtained in dry condition show that delamination wear was the predominant wear mechanism in the ER8 steel specimens. A stabilization of the damage is obtained after an initial run-in phase: this is confirmed by the wear curves, which highlight a stabilization of the wear rate, as well as by the surface damage indexes, which show that both the roughness and the general surface state detected by the vision systems tend to accommodate to a steady value. This observation is consistent with the behavior studied by Mazzù and Donzella [37], who numerically showed that under constant working condition, in dry contact, an equilibrium can reached between the accumulation of plastic strain (ratcheting) and wear, so that the material state both in the surface and in the subsurface layer appears constant and consistent with the strain field and surface cracks depicted in the experimental sections of Fig. 12. In that work, it was shown that the depth of the plasticized layer is determined by some material constants of the cyclic plasticity model which can be correlated to the material hardness: the harder the material, the lower the depth of the plasticized layer.

In this paper, a direct correlation was observed between the depth of the deformed layer and the wear rate of the samples (Fig. 15), with greater deformed layer depth being associated with increased mass loss. Similar findings were reported by other authors in twin-disc tests on various wheel steels [2,35,38], demonstrating that the extent of the deformed layer influences the wear rate. Therefore, both plasticization and wear rate appear well correlated with the material hardness, as well as the surface damage indexes shown in Fig. 10. The sum of all these data indicates that the specimen taken from the less deep layers, characterized by higher hardness and higher content of bainitic islands, are more resistant to delamination wear, which is the prevailing phenomenon in dry condition. This consideration aligns with the findings of Hu et al. [29], who reported that the wear rates of ER7, CL60 and class C wheel steels decreased with increasing steel hardness. Conversely, this is in contrast with the results of Li et al. [5] and Zhang et al. [6], who reported a detrimental effect of a high bainitic content with respect to a completely ferritic-pearlitic microstructure.

Concerning the work hardening behavior shown in Fig. 14, the results confirm those reported by Zhang et al. [39], who compared the plastic deformation behavior of ER8 steel with a microstructure consisting of pearlite (P), ferrite (F) and bainite (B) in an unspecified proportion to that of ER8 steel with a fully ferritic-pearlitic microstructure. The authors found that the deformation and work hardening of ER8 steel containing bainite were less pronounced than those of ER8 with a ferritic-pearlitic microstructure during the wear process. As a result, the P + F + B microstructure exhibited lower surface hardness at the end of bi-disc tests. However, again these findings are in contrast with those of Li et al. [5]. In their study, the authors measured a greater hardness increase in ER8 steel containing 50 % bainite compared to the same steel with a fully ferritic-pearlitic microstructure.

All these results can be interpreted in light of the work of Zani et al. [10], showing that the bainitic content can compromise both wear and RCF resistance only beyond approximately 11 %. Therefore, in the presence of bainite within the ferritic-pearlitic microstructure of ER8 steel, its amount is the key factor in determining resistance to wear and ratcheting: in low concentration, as is the case studied in this paper, it seems not a determinant factor in dry condition.

The content of bainitic islands, within the range investigated in this paper, seems an irrelevant parameter even in the wet phase of the mixed tests. In fact, the weight loss diagrams shown in Fig. 8 show a great dispersion of the data; even considering the averages, no correlation can be found with the bainite content. The cross-sections shown in Fig. 13 confirm that no substantial differences can be found between the different depth of extraction of the specimens.

These evidences lead to consider the bainitic content, in the low concentrations examined in this study, irrelevant in terms of resistance to both wear and RCF.

5. Conclusions

To address the lack of knowledge about the effect of dispersed bainitic islands as a remnant of the production process, an experimental campaign was made on an ER8 steel for railway wheels, using specimens extracted at four different depths under the tread of a raw wheel. As far as the depth of extraction increased, the hardness and the content of bainitic islands decreased, from approximately 12 %–0 %. The wheel specimens were tested in rolling and sliding contact against specimens extracted from a rail in 900A steel, both in fully dry condition, and in dry condition followed by wet contact. The damage on the wheel specimens was evaluated in terms of contact surface state, weight loss and subsurface plasticization and cracking.

The following main conclusions were drawn:

- In dry condition, the main damage mechanism is delamination wear; its severity increases as far as the depth of extraction of the specimens increases, being correlated to the material hardness.
- In wet condition, the main damage mechanism is shelling, which is caused by the propagation of surface cracks previously formed by

ratcheting in the dry phase; no clear correlation with the depth of extraction can be identified.
- The content of bainitic islands, in the low concentrations studied in this work, appears an irrelevant factor in the resistance to wear and RCF.

This leads to conclude that pushing towards a zero bainite content can be counterproductive, because to obtain such result an excessively thick allowance has to be removed, this way wasting the most performant layers in terms of wear and RCF resistance. Conversely, tolerating a small content of bainite islands, which do not affect the material performances, seems the best compromise choice.

CRediT authorship contribution statement

Angelo Mazzù: Writing – original draft, Methodology, Investigation, Data curation, Conceptualization. **Nicola Zani:** Methodology, Investigation, Data curation. **Candida Petrogalli:** Methodology, Investigation, Data curation. **Ileana Bodini:** Methodology, Investigation, Data curation. **Lorenzo Ghidini:** Writing – review & editing, Methodology, Investigation, Data curation, Conceptualization. **Michela Faccoli:** Writing – review & editing, Methodology, Investigation, Data curation, Conceptualization.

Declaration of competing interest

The authors declare that they have no known competing financial interests or personal relationships that could have appeared to influence the work reported in this paper.

Data availability

Data will be made available on request.

References

[1] A. Ghidini, M. Diener, A. Mazzù, N. Zani, C. Petrogalli, M. Faccoli, Considerations about microstructure of solid wheels with traces of bainite | Considerazioni sulla microstruttura di ruote monoblocco con tracce di bainite, Ing. Ferrov. 75 (2020) 165–178.

[2] R.S. Miranda, A.B. Rezende, S.T. Fonseca, F.M. Fernandes, A. Sinatora, P.R. Mei, Fatigue and Wear Behavior of Pearlitic and Bainitic Microstructures with the Same Chemical Composition and Hardness Using Twin-Disc Tests, Wear, 2022, pp. 494–495, https://doi.org/10.1016/j.wear.2022.204253.

[3] T. Zhou, H. Xu, X. Ma, Z. Xu, H. Zhao, Y. He, A novel carbide-free bainitic heavy-haul wheel steel with an excellent wear-resistance under rolling-sliding condition, Metals 13 (2023), https://doi.org/10.3390/met13020202.

[4] S. Sharma, S. Sangal, K. Mondal, Wear behavior of newly developed bainitic wheel steels, J. Mater. Eng. Perform. 24 (2015) 999–1010, https://doi.org/10.1007/s11665-014-1328-6.

[5] Q. Li, J. Guo, A. Zhao, Effect of upper bainite on wear behaviour of high-speed wheel steel, Tribol. Lett. 67 (2019), https://doi.org/10.1007/s11249-019-1239-7.

[6] B. Gao, Z. Tan, Z. Liu, G. Gao, M. Zhang, G. Zhang, B. Bai, Influence of non-uniform microstructure on rolling contact fatigue behavior of high-speed wheel steels, Eng. Fail. Anal. 100 (2019) 485–491, https://doi.org/10.1016/j.engfailanal.2019.03.002.

[7] G.-Z. Zhang, C.-P. Liu, H. Zhang, Q. Li, R.-M. Ren, Study on wear properties of J11 wheel steel with nonuniform microstructure, J. Mater. Eng. Perform. 29 (2020) 7420–7427, https://doi.org/10.1007/s11665-020-05183-0.

[8] O.I. Babachenko, G.A. Kononenko, R.V. Podolskyi, O.A. Safronova, O.L. Safronov, Z.A. Dementiev, Study of correlation of chemical and phase composition and fracture toughness of railway wheel steel, Mater. Sci. 60 (2024) 33–38, https://doi.org/10.1007/s11003-024-00847-x.

[9] C. Suetrong, V. Uthaisangsuk, Investigations of fatigue crack propagation in ER8 railway wheel steel with varying microstructures, Mater. Sci. Eng., A 840 (2022), https://doi.org/10.1016/j.msea.2022.142980.

[10] N. Zani, T. Chaise, A. Ghidini, M. Faccoli, A. Mazzù, Numerical study about the effect of bainitic traces on plasticity in ferritic-pearlitic railway wheels, Proc. Inst. Mech. Eng. F J. Rail Rapid Transit 235 (2021) 726–740, https://doi.org/10.1177/0954409720960888.

[11] G. Donzella, M. Faccoli, A. Mazzù, C. Petrogalli, R. Roberti, Progressive damage assessment in the near-surface layer of railway wheel-rail couple under cyclic contact, Wear 271 (2011), https://doi.org/10.1016/j.wear.2010.10.042.

[12] A. Mazzù, C. Petrogalli, M. Faccoli, An integrated model for competitive damage mechanisms assessment in railway wheel steels, Wear (2015) 322–323, https://doi.org/10.1016/j.wear.2014.11.013.

[13] A. Mazzù, L. Solazzi, M. Lancini, C. Petrogalli, A. Ghidini, M. Faccoli, An experimental procedure for surface damage assessment in railway wheel and rail steels, Wear (2015) 342–343, https://doi.org/10.1016/j.wear.2015.08.006.

[14] M. Faccoli, C. Petrogalli, M. Lancini, A. Ghidini, A. Mazzù, Rolling contact fatigue and wear behavior of high-performance railway wheel steels under various rolling-sliding contact conditions, J. Mater. Eng. Perform. 26 (2017), https://doi.org/10.1007/s11665-017-2786-4.

[15] A. Mazzù, C. Petrogalli, M. Lancini, A. Ghidini, M. Faccoli, Effect of wear on surface crack propagation in rail–wheel wet contact, J. Mater. Eng. Perform. (2018), https://doi.org/10.1007/s11665-018-3185-1.

[16] A. Mazzu, I. Bodini, N. Zani, L. Ghidini, C. Petrogalli, S. Bonometti, G. Coffetti, D. Palandi, Surface damage assessment in rail and wheel steels using an innovative vision system, in: J. Pombo (Ed.), Proceedings of the Sixth International Conference on Railway Technology: Research, Development and Maintenance, Civil-Comp Press, Edinburgh, 2024, pp. 1–13, https://doi.org/10.4203/ccc.7.9.4.

[17] I. Bodini, A. Mazzù, C. Petrogalli, M. Lancini, T. Kato, T. Makino, A study of wear and rolling contact fatigue on a wheel steel in alternated dry-wet contact aided by innovative measurement systems, in: Procedia Structural Integrity, 2019, pp. 849–857, https://doi.org/10.1016/j.prostr.2019.08.235.

[18] I. Bodini, N. Zani, C. Petrogalli, A. Mazzù, T. Kato, T. Makino, Damage assessment in a wheel steel under alternated dry-lubricated contact by an innovative vision system, Wear (2023) 530–531, https://doi.org/10.1016/j.wear.2023.205064.

[19] I. Bodini, C. Petrogalli, A. Mazzù, S. Pasinetti, T. Kato, T. Makino, A vision-based approach for rolling contact fatigue evaluation in twin-disc tests on a railway wheel steel, Tribology - materials, Surf. Interfaces 15 (2021) 92–101, https://doi.org/10.1080/17515831.2020.1825062.

[20] I. Bodini, C. Petrogalli, M. Faccoli, M. Lancini, S. Pasinetti, G. Sansoni, F. Docchio, A. Mazzù, Evaluation of wear in rolling contact tests by means of 2D image analysis, Wear 400–401 (2018) 156–168, https://doi.org/10.1016/j.wear.2017.12.023.

[21] R. Lewis, R.S. Dwyer-Joyce, Wear mechanisms and transitions in railway wheel steels, Proc. IME J. J. Eng. Tribol. 218 (2004) 467–478, https://doi.org/10.1243/1350650042794815.

[22] R. Lewis, U. Olofsson, Mapping rail wear regimes and transitions, Wear 257 (2004) 721–729, https://doi.org/10.1016/j.wear.2004.03.019.

[23] D.H. Mesa G, I.A. Vásquez-Chacón, M.A. Gómez–Guarneros, P. Sanchez-Tizapantzi, E.A. Gallardo-Hernández, A pin-on-disk wear map of rail and wheel materials from different standards, Mater. Lett. 307 (2022), https://doi.org/10.1016/j.matlet.2021.131021.

[24] T. Jendel, Prediction of wheel profile wear - comparisons with field measurements, Wear 253 (2002) 89–99, https://doi.org/10.1016/S0043-1648(02)00087-X.

[25] G. Donzella, M. Faccoli, A. Ghidini, A. Mazzù, R. Roberti, The competitive role of wear and RCF in a rail steel, Eng. Fract. Mech. 72 (2005), https://doi.org/10.1016/j.engfracmech.2004.04.011.

[26] J.W. Ringsberg, Shear mode growth of short surface-breaking RCF cracks, Wear 258 (2005) 955–963, https://doi.org/10.1016/j.wear.2004.03.043.

[27] L. Ma, C.G. He, X.J. Zhao, J. Guo, Y. Zhu, W.J. Wang, Q.Y. Liu, X.S. Jin, Study on wear and rolling contact fatigue behaviors of wheel/rail materials under different slip ratio conditions, Wear (2016) 366–367, https://doi.org/10.1016/j.wear.2016.04.028, 13–26.

[28] C.-P. Liu, R.-M. Ren, D.-Y. Liu, X.-J. Zhao, C.-H. Chen, An EBSD investigation on the evolution of the surface microstructure of D2 wheel steel during rolling contact fatigue, Tribol. Lett. 68 (2020), https://doi.org/10.1007/s11249-020-1277-1.

[29] Y. Hu, L. Zhou, H.H. Ding, R. Lewis, Q.Y. Liu, J. Guo, W.J. Wang, Microstructure evolution of railway pearlitic wheel steels under rolling-sliding contact loading, Tribol. Int. 154 (2021), https://doi.org/10.1016/j.triboint.2020.106685.

[30] N.P. Suh, The delamination theory of wear, Wear 25 (1973) 111–124, https://doi.org/10.1016/0043-1648(73)90125-7.

[31] S. Bogdariski, P. Lewicki, M. Szymaniak, Experimental and theoretical investigation of the phenomenon of filling the RCF crack with liquid, Wear 258 (2005) 1280–1287, https://doi.org/10.1016/j.wear.2004.03.038.

[32] F. Khalil, M. Kavoosi, Effect of Lubricant on Surface Rolling Contact Fatigue Cracks, 2010. https://doi.org/10.4028/www.scientific.net/AMR.97-101.793.

[33] A.F. Bower, Influence of crack face friction and trapped fluid on surface initiated rolling contact fatigue cracks, in: American Society of Mechanical Engineers (Paper), 1988.

[34] A. Ghidini, M. Diener, A. Gianni, J. Schneider, SUPERLOS innovative steel by Lucchini RS for high-speed wheel application, Lucchini RS, LRS-Techno Series 5 (2012) 82–116.

[35] A.B. Rezende, S.T. Fonseca, F.M. Fernandes, R.S. Miranda, F.A.F. Grijalba, P.F. S. Farina, P.R. Mei, Wear behavior of bainitic and pearlitic microstructures from microalloyed railway wheel steel, Wear (2020) 456–457, https://doi.org/10.1016/j.wear.2020.203377.

[36] H. Yokoyama, S. Mitao, S. Yamamoto, Wear and Rolling Contact Fatigue behavior in pearlitic and bainitic rail steels, in: Proceedings of the 7th International Heavy Haul Conference, International Heavy Haul Association, Brisbane, Australia, 2001, pp. 10–14. June, 2001.

[37] A. Mazzù, G. Donzella, A model for predicting plastic strain and surface cracks at steady-state wear and ratcheting regime, Wear 400–401 (2018) 127–136, https://doi.org/10.1016/j.wear.2018.01.002.
[38] C.G. He, J. Guo, Q.Y. Liu, W.J. Wang, Experimental investigation on the effect of operating speeds on wear and rolling contact fatigue damage of wheel materials, Wear (2016) 364–365, https://doi.org/10.1016/j.wear.2016.08.006, 257–269.
[39] G.-Z. Zhang, C.-P. Liu, R.-M. Ren, S. Wu, H.-X. Yin, T. Cong, X. Li, Effect of nonuniform microstructure on wear property of ER8 wheel steel, Wear (2020) 458–459, https://doi.org/10.1016/j.wear.2020.203416.